applied sciences

MDPI

Article

Analysis of Time-Domain Shielding Effectiveness of Lightweight Metallized Carbon Fiber Composite Chassis

Le Cao [1], Cheng-Zhi Yuan [1], Hao-Wei Yuan [1], Guang-Hui Du [1], Tian-Yi Zhang [2] and Xu-Qing Liu [2,*]

[1] School of Electric and Control Engineering, Xi'an University of Science and Technology, Xi'an 710054, China; caole@xust.edu.cn (L.C.); 22206029011@stu.xust.edu.cn (C.-Z.Y.); 21206029012@stu.xust.edu.cn (H.-W.Y.); duguanghui@xust.edu.cn (G.-H.D.)

[2] Center of Advanced Lubrication and Seal Materials, State Key Laboratory of Solidification Processing, Northwestern Polytechnical University, Xi'an 710072, China; tianyizhang@mail.nwpu.edu.cn

* Correspondence: xqliu@nwpu.edu.cn

Abstract: Electromagnetic interference poses a significant challenge to the reliability and performance of electronic equipment, particularly in the aerospace and aviation sectors where the demand for high-performance electromagnetic shielding materials is paramount. This study introduces an innovative solution: a lightweight nickel-plated carbon fiber composite chassis, designed to meet these stringent requirements. Through comparative analysis, we prove that this composite chassis is not only comparable to traditional metal chassis in terms of time-domain shielding effect, but also close to traditional metal chassis in terms of heat dissipation capability. Notably, it achieves a substantial weight reduction of 71.43% to 76.25% compared to its metal counterparts, addressing the critical need for lighter materials in aerospace applications. The superior heat dissipation feature of the nickel-plated carbon fiber composite, quantitatively superior to conventional materials, indicates its potential to enhance the operational efficiency and safety of aerospace electronics. This research underscores the viability of nickel-plated carbon fiber composites as a groundbreaking material for electromagnetic shielding, promising significant advancements in aerospace and beyond.

Keywords: time-domain shielding effectiveness; composite materials; thermal analysis; lightweight chassis

check for updates

Citation: Cao, L.; Yuan, C.-Z.; Yuan, H.-W.; Du, G.-H.; Zhang, T.-Y.; Liu, X.-Q. Analysis of Time-Domain Shielding Effectiveness of Lightweight Metallized Carbon Fiber Composite Chassis. *Appl. Sci.* **2024**, *14*, 4361. https://doi.org/10.3390/app14114361

Academic Editor: Giuseppe Lacidogna

Received: 25 March 2024
Revised: 13 May 2024
Accepted: 19 May 2024
Published: 21 May 2024

Copyright: © 2024 by the authors. Licensee MDPI, Basel, Switzerland. This article is an open access article distributed under the terms and conditions of the Creative Commons Attribution (CC BY) license (https://creativecommons.org/licenses/by/4.0/).

1. Introduction

With the widespread use of electronic devices in recent years, electromagnetic pulse (EMP) protection technology for electronic devices has received extensive attention. In the realm of electrical engineering, EMP interference presents a formidable challenge, impacting the functionality of electronic devices and, in severe instances, leading to irreversible damage to such equipment [1,2]. To mitigate the adverse effects of EMP on electronic systems and apparatus, the deployment of shielding chassis has become a standard practice within the engineering domain [3–5]. Lightweight portable chassis are widely used, such as for small portable radar chassis, for the shielding body of important electronic equipment for aircraft and vehicles, and for small metal square cabins. For most portable electronic devices, shielding enclosures can significantly increase the overall size and weight of the electronic device. As a result, shielding cavities generally have holes and slots for heat dissipation, wiring, and splicing. However, these holes and slots also become important paths for electromagnetic wave coupling into electronic devices, thus reducing the shielding effect [6–8]. Therefore, in scenarios where lightweight shielding materials are required, such as in the aerospace field, a lightweight EM shielding chassis with both shielding performance and heat dissipation is needed.

Historically, materials such as copper, aluminum, and stainless steel have been the mainstays for constructing shielding chassis, selected for their satisfactory electromagnetic shielding attributes [9–12]. However, the high density and weight of these materials

limit their application in electromagnetic shielding fields, given the need for lightweight shielding chassis. Carbon fiber, with its mechanical robustness and low density, gives it great potential for manufacturing shielded enclosures. Unfortunately, the electromagnetic shielding performance of carbon fiber fails to reach the standard [13,14]. Recent advancements have illuminated the potential of composite materials to significantly augment the electromagnetic shielding efficacy of structures while preserving the intrinsic properties of the base materials [15–19]. Noteworthy contributions to this field include the work of Savi, P et al. [15], who explored the shielding effectiveness of biocarbon-based coatings under varying incidence conditions. Similarly, Yoo, J et al. [16] prepared a flexible and elastic Fe-based amorphous soft magnetic composite for shielding against harmful electromagnetic waves in industrial and military defense applications. Zhang, X.Z et al. [17] investigated the in situ growth of carbon nanotubes on slag using polymer pyrolytic chemical vapor deposition (PP-CVD) to improve the electromagnetic interference shielding of cementitious composites. Further, Juan Chen et al. [18] found that rGO-CF was more effective than CF in improving the electromagnetic interference (EMI) shielding performance of unsaturated polyester-based composites by introducing graphene oxide onto the surface of carbon fibers and then reducing the graphene oxide flakes on the carbon fibers with NaBH4 solution. Amaro, A et al. [19] examined the role of carbon nanotube concentration on the dispersion within polymer matrices and the consequent effects on the shielding capabilities of carbon nanotube–polyolefin composites. These studies fully support the considerable prospects and development potential of composites in the field of electromagnetic shielding.

Furthermore, the traditional evaluation of electromagnetic shielding is based on the frequency domain, which provides a standard for evaluating the protective performance of chassis, and electromagnetic shielding technology has developed rapidly under this standard. Yet, the advent of high-power EMP technologies has spotlighted the limitations inherent in frequency-domain analysis, particularly in the context of robust EMP threats. The strong demand for electromagnetic shielding under high-power EMP conditions has led to widespread interest in time-domain shielding effectiveness (TDSE), and this demand highlights the value of time-domain SE (TDSE) analysis, which provides a more detailed characterization of the shielding capability of a chassis under EMP conditions than when assessed using only frequency-domain SE [8]. The significance of TDSE analysis in enhancing our understanding and development of effective shielding solutions cannot be overstated, marking a critical area of research in electromagnetic protection.

In conclusion, it is of great importance to develop shielding chassis with both good shielding performance and heat dissipation in aerospace and other areas where lightweight is required. In addition, frequency-domain SE is not sufficient in the analysis of shielding performance under high-power EMP illumination, and time-domain SE should be introduced. To solve the above problems, the following work is conducted in this study:

(1) The development of a nickel-plated carbon fiber composite is introduced, and its electromagnetic parameters (including dielectric constant and permeability) are characterized.
(2) A chassis model with holes and slots is established. Then, the electric fields at different observation points inside the three kinds of material (metal, carbon fiber, and nickel-plated carbon fiber) chassis are analyzed by the time-domain difference (FDTD) method. Finally, the TDSEs for the three kinds of chassis are calculated and compared.
(3) The thermal dissipation characteristics of the three chassis are critically evaluated using COMSOL Multiphysics 6.1 software.

The rest of this paper is organized as follows. In Section 2, the overall method is described, including the preparation and measurement of the composite material and the computing method of the proposed chassis. In Section 3, the electric fields and TDSE of the novel chassis are computed and analyzed, and heat dissipation of the chassis is given. Finally, the conclusions are presented in Section 4.

2. Methodology

In this study, a metalized carbon fiber composite material is developed, and a lightweight electromagnetic shielding chassis is designed using this material. Using the FDTD method and COMSOL software, the TDSE and heat dissipation performance of the chassis with different materials are simulated, and the comprehensive performance of the chassis with three different materials is compared.

First, the nickel-plated carbon fiber composite is prepared, which was initially undertaken through an electroless deposition process. Following this, the essential task of calculating the SE involved the meticulous measurement of the complex permittivity and magnetic permeability. These critical electromagnetic parameters were accurately determined using a vector network analyzer, ensuring the reliability of the subsequent analyses. Subsequently, the architecture of the composite chassis was modeled to facilitate a comprehensive examination of electromagnetic field distributions within the structure. This modeling enabled the precise identification of field values at strategically placed observation points inside the chassis, achieved through the application of 3D-FDTD iterative calculations. The utilization of the FDTD method allowed for the extraction of time-domain SE metrics, providing a nuanced understanding of the chassis's shielding capabilities. Expanding upon this foundation, the study delved deeper into the nuanced analysis of the composite chassis's time-domain SE under a variety of test conditions. These conditions encompassed differing angles of incidence and polarization, alongside a spectrum of polarization modes, thereby offering a robust evaluation of the chassis's performance across diverse electromagnetic scenarios. Each scenario was meticulously designed to mimic realistic operational environments, thus ensuring the applicability of the findings. Finally, COMSOL software was used to analyze the heat dissipation rates of metal chassis, carbon fiber chassis, and composite chassis to fully evaluate the comprehensive performance of the shielding chassis proposed in this paper. Illustrative of the methodological approach, Figure 1 encapsulates the flow of the study, delineating each step from the preparation of the composites to the final analysis of time-domain SE.

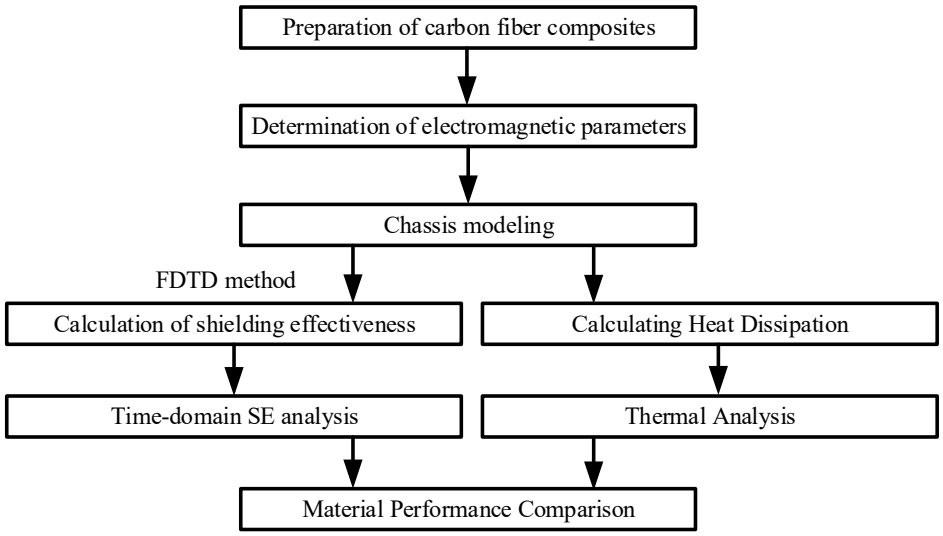

Figure 1. Research flowchart.

2.1. Preparation of the Composite Material

2.1.1. Preparation of Nickel-Plated Carbon Fibers

Initially, carbon fibers were immersed in an acetone solution and subjected to 60 min of ultrasonic cleaning to remove impurities, followed by rinsing and drying with deionized water. Subsequently, 50 mL of anhydrous ethanol was mixed with deionized water, into which 5 g of tannic acid was introduced and the carbon fibers were immersed for a period of 12 h. Following another cycle of washing and drying, the treated carbon fibers were

immersed in an ammonium chloropalladate catalyst solution, composed of 140 mg of ammonium chloropalladate in 40 mL of water, for 6 h. The carbon fibers were then gently rinsed in a slow stream of water, placed in a plating solution comprising 40 mL of Solution A and 10 mL of Solution B, with an additional 3 mL of ammonia. Solution A was prepared by dissolving 64 g of nickel sulphate hexahydrate, 32 g of sodium citrate, and 16 g of lactic acid in 400 mL of deionized water and stirring thoroughly. Solution B involved the addition of 240 mg of DMAB (dimethylamine borane) to 40 mL of water. The duration of immersion in the plating solution was adjusted based on the required thickness of the coating [20].

2.1.2. Fabrication of Nickel-Plated Carbon Fiber Composites

In a separate procedure, epoxy resins JC-02A and curing agent JC-02B were blended in a weight ratio of 100:85. The nickel-plated carbon fibers and the epoxy resin mixture were then combined using a vacuum-assisted resin transfer molding (VARTM) process. This involved three key steps: positioning the nickel-plated carbon fibers within the mold, injecting the resin into the mold, and heating the assembly in an oven. The curing regimen for the epoxy resin was set at 90 °C for 2 h, 110 °C for 1 h, and finally 130 °C for 6 h. Upon completion of this process, the nickel-plated carbon fiber composites were successfully produced.

2.1.3. Material Characterization

The characterization of the microstructural morphology of materials is crucially facilitated by the use of scanning electron microscopy (SEM), which operates on the principle of bombarding the material's surface with high-speed electrons emitted from an electron gun. This interaction generates a variety of electron signals, including backscattered electrons, secondary electrons, Auger electrons, and transmitted electrons. By collecting and amplifying these signals, SEM allows for the imaging and subsequent display of the material's three-dimensional real image on a fluorescent screen, thus achieving the goal of characterizing the microscopic morphology of substances. In the context of this study, flake samples were adhered to conductive adhesive for imaging, while powder specimens were dispersed in ethanol and subsequently dropped onto a silicon wafer for capture. The SEM utilized was the Helios G4 CX model from FEI Company, Hillsboro, OR, USA, with an acceleration voltage range of 200 V to 30 kV, catering to the diverse requirements of material imaging.

2.2. Determination of Electromagnetic Parameters of Composite Materials

The dielectric properties of the materials were tested using the waveguide method. This assessment was conducted on an MS4644A Vector Network Analyzer (VNA) produced by Anritsu, Atsugi, Japan. The waveguide method, commonly applied within the X-band frequency range of 8.2 GHz to 12.4 GHz, necessitates sample planes measuring 22.86 mm by 10.16 mm. To evaluate the dielectric properties across different frequency bands, varying sample sizes are required, the material surfaces were meticulously polished, cleaned, and dried to ensure accurate and reliable measurement results.

Upon the completion of this calibration phase, a coaxial transmission line was adjoined to an apparatus containing the sample material, facilitating the transmission of a microwave signal from the source. This configuration allowed for the signal to be conveyed directly to the sample via the coaxial line. Upon interacting with the sample, the signal was then rerouted back through the transmission line to the receiver. It was at this juncture that the VNA played a pivotal role, meticulously tracking, processing, and cataloguing the signals and their fluctuations, culminating in the visualization of the data on a computer system. This process effectively completed the acquisition of scattering parameter (S-parameter) data, a critical step in our analysis.

The gathered S-parameters were then rigorously applied to Equations (1) and (2), facilitating the computation of the complex permittivity and permeability of the nickel-plated carbon fiber. This methodical approach not only ensured the precision of our measurements but also provided a comprehensive understanding of the material's electromagnetic

characteristics. Through this sophisticated analytical procedure, we were able to derive invaluable insights into the dielectric properties of the nickel-plated carbon fiber materials, thereby contributing significantly to our knowledge base in the field of electromagnetic material science.

$$\varepsilon = \frac{\frac{1}{kd}\cos^{-1}\left[\frac{1}{2S_{21}}(1 - S_{11}^2 + S_{21}^2) + 2\pi m\right]}{\sqrt{\frac{(1-S_{11})^2 - S_{21}^2}{(1+S_{11})^2 - S_{21}^2}}} \tag{1}$$

$$\mu = \frac{1}{kd}\cos^{-1}\left[\frac{1}{2S_{21}}(1 - S_{11}^2 + S_{21}^2) + 2\pi m\right]\sqrt{\frac{(1+S_{11})^2 - S_{21}^2}{(1-S_{11})^2 - S_{21}^2}} \tag{2}$$

2.3. Chassis Modeling

The model of the double-layer shielding chassis containing hole and slit structures is shown in Figure 2, where the front of the chassis is the plane where the holes and slits are located parallel to the zoy-plane of the coordinate system; the total dimensions of the chassis are 170 mm × 130 mm × 60 mm; the thickness is 3 mm, in which the dimensions of the outer shielding cavity are 170 mm × 50 mm × 60 mm; and the dimensions of the inner shielding cavity are 170 mm × 80 mm × 60 mm. There are two rows of rectangular hole arrays on the inner and outer shielding cavities, and the size of each rectangular hole is 15 mm × 7 mm. The three arrangements of the hole arrays of the inner shielding cavity are shown in Figure 3, which are "Horizontal–Vertical", "Horizontal–Horizontal", and "Vertical–Vertical". The hole array arrangement of the chassis and the chassis numbering are shown in Table 1. The observation point is set at the center of the inner shielding cavity. The electromagnetic wave is incident from the front of the chassis with aperture slits. The incident wave is a double-exponential pulse, which can be written as follows:

$$E = AE_0[\exp(-at) - \exp(-bt)] \tag{3}$$

where E_0 = 50 kV/m, $A = 1.3$, $a = 1.0 \times 10^9$ s, and $b = 1.5 \times 10^{10}$ s; where E_0 is the peak field strength, A is the peak pulse correction factor, and a and b are pulse parameters.

For the numerical electromagnetic model, there are four types of media included in the calculation grid: vacuum, carbon fiber, nickel-plated carbon fiber, and stainless steel. The total number of grids is 190 × 150 × 80. The discrete grid in the FDTD calculation is $\delta = 1 \times 10^{-3}$ m. As we know, the time step size is $\Delta t = 0.00167$ ns. The CPML absorbing boundary is employed in the FDTD calculation. The connecting surface boundary is −98:98 (x-direction); −78:78 (y-direction); and −43:43 (z-direction). The absorbing boundary is −108:108 (x-direction); −88:88 (y-direction); and −53:53 (z-direction).

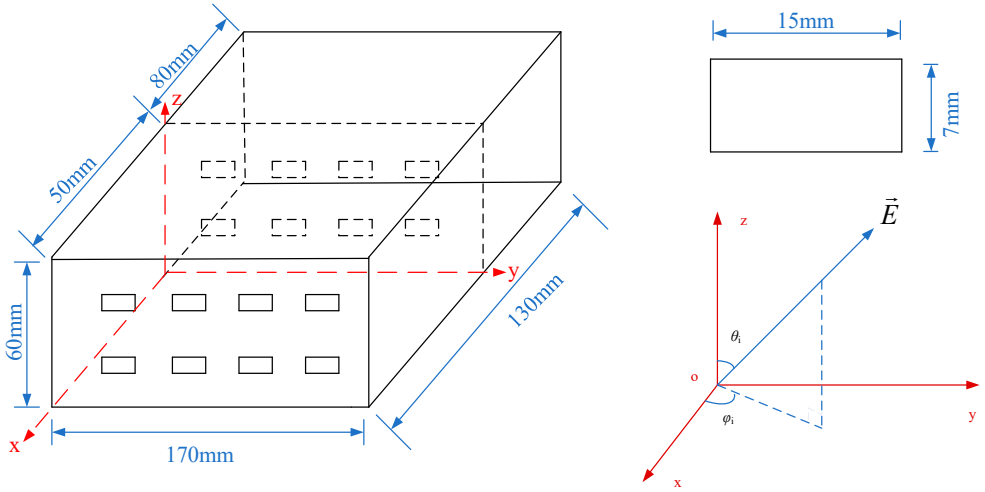

Figure 2. Diagram of chassis structure.

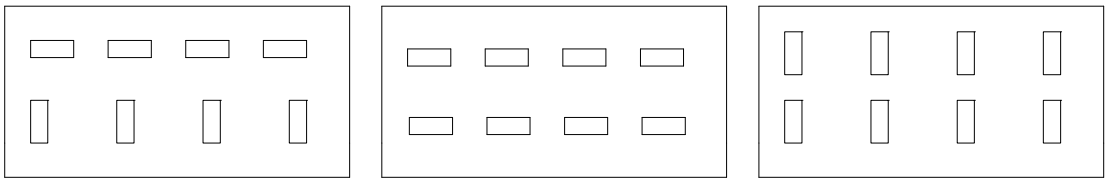

(a) (b) (c)

Figure 3. Three arrangements of hole arrays: (**a**) Horizontal–Vertical; (**b**) Horizontal–Horizontal; (**c**) Vertical–Vertical.

Table 1. Arrangement of hole array and corresponding number.

Chassis Number	Arrangement of Holes in the Outer Shield	Arrangement of Holes in the Inner Shield
chassis 1	Horizontal–Horizontal	Horizontal–Horizontal
chassis 2	Horizontal–Horizontal	Horizontal–Vertical
chassis 3	Horizontal–Horizontal	Vertical–Vertica

2.4. Definition of Time-Domain Shielding Effectiveness

The swift advancement in high-intensity EMP technology reveals that assessing shielding performance solely based on frequency-domain shielding effectiveness presents notable limitations in gauging the protective capability against potent EMPs. Consequently, the evaluation of a material's or structure's resilience to strong electromagnetic pulses is more accurately conducted through time-domain shielding effectiveness measurements.

Generally, most electronic devices are sensitive to one or more of the following physical quantities: the maximum value of the electric field $E_{\max}$, the maximum value of induced effects caused by the time variations in electric flux density $\dot{E}_{\max}$, and the total energy delivered W. Accordingly, there are three definitions of TDSE [21]:

Peak-value-reduction SE:

$$SE_{PR} = 20 \times \lg(E_{0-\max}/E_{s-\max}) \tag{4}$$

Derivative-reduction SE:

$$SE_{DR} = 20 \times \lg\left(\dot{E}_{0-\max}/\dot{E}_{s-\max}\right) \tag{5}$$

Energy-density-reduction SE:

$$SE_{WR} = 10 \times \lg(W_0(x,y,z)/W_s(x,y,z)) \tag{6}$$

where the subscript "0" represents the value of the electric field at the observation point in the absence of the enclosure. When the enclosure is present, we use the subscript "s". In practical testing, the peak field strength emerges as the most straightforward parameter to gauge, leading to its prevalent use in evaluating the TDSE of a shielding material.

3. Results and Discussions

3.1. Mophorlogy of Metal-Coated Fibers

Figure 4 presents SEM images that illustrate the uniform and compact deposition of nickel on a carbon fiber surface, highlighting the tight packing of nickel particles to form a continuous, dense layer across the fiber. Figure 4a depicts the extensive coverage of nickel particles, essential for creating a conductive path that enhances electromagnetic shielding properties. Figure 4b, derived from the nickel elemental distribution map associated with Figure 4a, confirms the uniform distribution of nickel across the fiber, indicating a consistent shielding effectiveness essential for electromagnetic protection. Figure 4c, a high-magnification SEM image, offers a detailed look at the tightly interconnected nickel

particles, showing no visible gaps and particle diameters ranging from 0.5 to 1 µm. This compact layer is crucial for improving the material's effectiveness in blocking electromagnetic interference, showcasing the effectiveness of the electroless deposition process in achieving a nickel-coated carbon fiber with superior electromagnetic shielding capabilities and structural integrity.

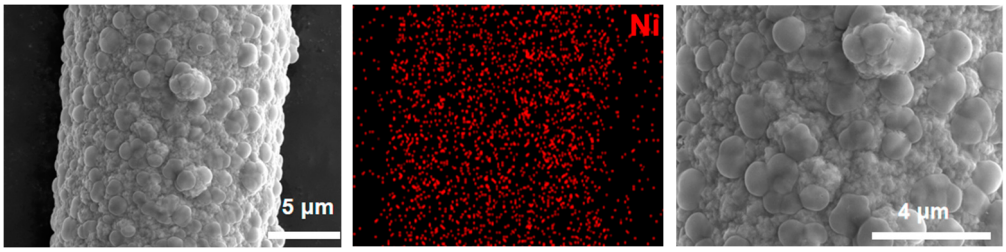

Figure 4. The morphology of fibers pre- and post-electroless nickel plating: (**a**) carbon fiber; (**b**) nickel-plated carbon fiber; (**c**) High-Magnification SEM Image of Compact Nickel Particles.

3.2. Dielectric Constant and Permeability of Composites

The electromagnetic parameters of the nickel-plated carbon fiber in the X-band are shown in Figure 5, where Figure 5a shows the complex permittivity of the nickel-plated carbon fiber, Figure 5b shows the complex permeability, Figure 5c shows the tangent of the dielectric loss angle, and Figure 5d shows the tangent of the magnetic loss angle. EM(R) and EM(I) are the real and imaginary parts of the complex dielectric constant, and MU(R) and MU(I) are the real and imaginary parts of the complex permeability, respectively.

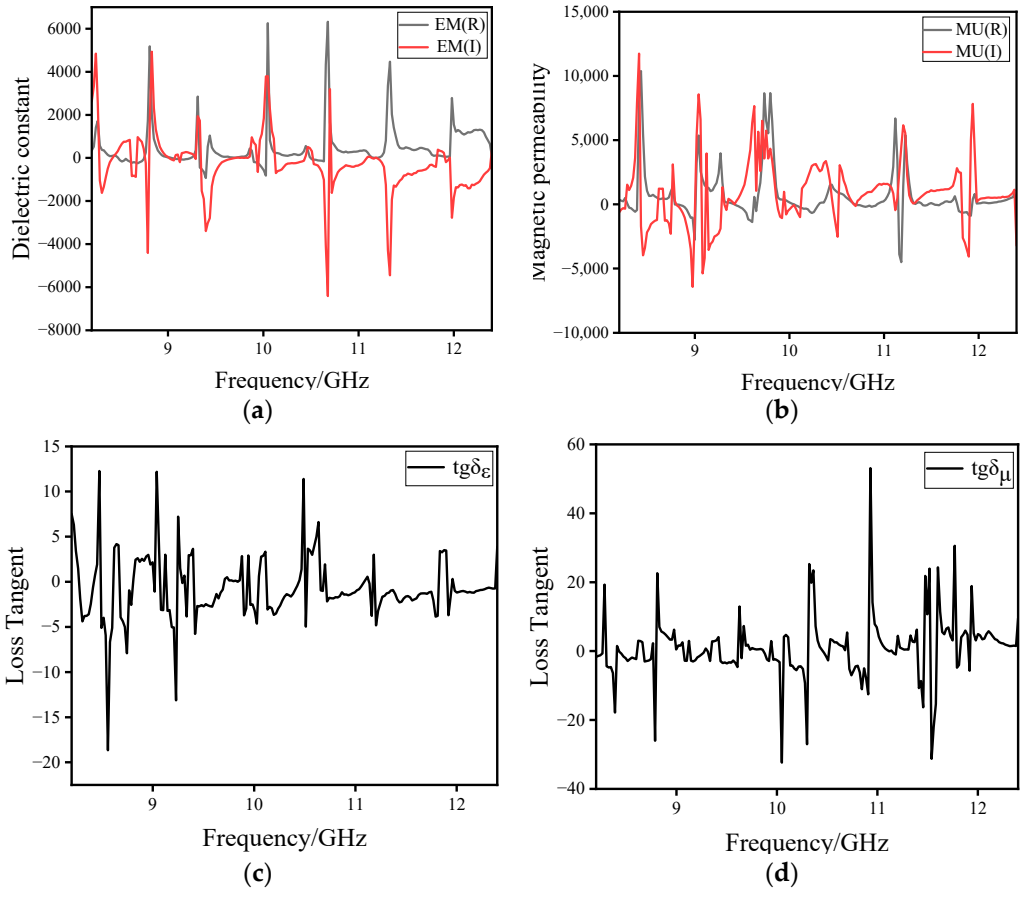

Figure 5. Electromagnetic parameters of nickel-plated carbon fibers: (**a**) dielectric constant; (**b**) permeability; (**c**) tangent of the dielectric loss angle; (**d**) tangent of the magnetic loss angle.

3.3. Time-Domain SE of Different Materials

Figure 6 shows the calculated electric field at observation point in chassis 2 under different polarization modes, with the angle of the incident wave set as $\varphi_i = 0°$ and $\theta_i = 90°$, respectively. Figure 6a is the result of the calculation of the horizontal polarization, and Figure 6b is the vertical polarization.

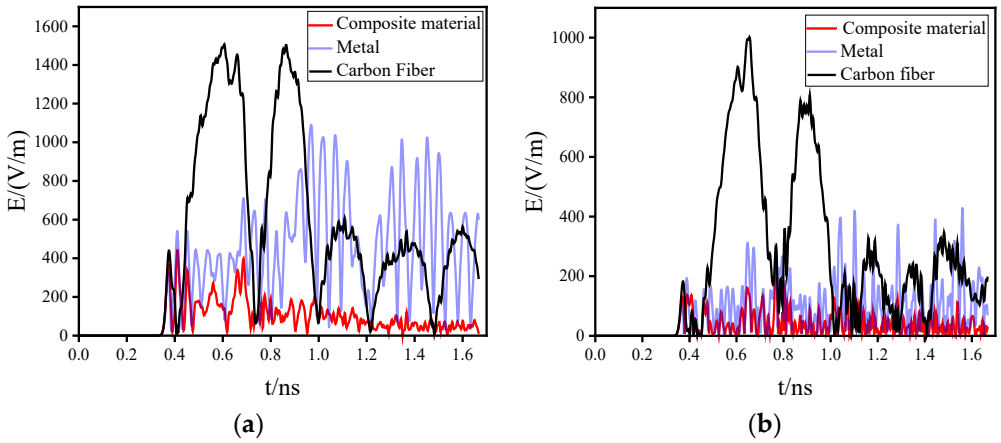

Figure 6. Variation in electric field with time at the chassis observation point: (**a**) horizontal polarization; (**b**) vertical polarization.

The results show that the electric fields at the observation points are different for all three materials under different polarization modes. It can be seen that the peak electric field at the observation point in the carbon fiber chassis is the highest and the TDSE is the lowest, regardless of vertical or horizontal polarization. The peak electric field of the metal chassis is smaller than that of the carbon fiber chassis and larger than that of the nickel-plated carbon fiber chassis. This is because when electromagnetic waves are coupled into the chassis, the high conductivity of the stainless steel generates a strong impedance mismatch with the air, resulting in strong reflected waves. For nickel-plated carbon fiber chassis, the high conductivity of the outermost layer of nickel can effectively reflect electromagnetic waves. At the same time, from the inside of the chassis to the outside of the formation of an "air–carbon fiber–nickel" structure, this conductivity gradient increases the asymmetric structure and can effectively improve the impedance mismatch problem to alleviate the reflection of electromagnetic waves inside the chassis. Finally, the nickel-plated layer has good magnetic properties, which can further absorb the electromagnetic wave reflected to the nickel-plated layer inside the chassis. Thus, the peak electric field inside the chassis decreases significantly. Therefore, the nickel-plated carbon fiber chassis has the highest time-domain shielding effectiveness.

To further illustrate the advantages of nickel-plated carbon fiber materials, we performed simulations in a double-layer shielded chassis with different aperture array structures. The aperture arrays on the inner shielding chambers are set according to Table 1, and the calculation results are shown in Figure 7, where Figure 7a shows the calculation results for horizontal polarization and Figure 7b shows the calculation results for vertical polarization.

As can be seen in Figure 7, the peak electric field is reduced at each observation point, which proves the good shielding performance of the composite. The comparative SE_{PR} of each material's chassis, as a function of varying different hole array structures and polarization modes, are systematically tabulated in Table 2. Additionally, to contextualize the relative weights of the three materials' chassis, their densities are enumerated within the table, where α denotes the polarization angle. From Table 3, it can be seen that the time-domain shielding effectiveness of the nickel-plated carbon fiber double-layer shielding chassis is better than that of the carbon fiber double-layer shielding chassis and the metal double-layer shielding chassis, and in terms of weight, the weight reduction of the nickel-

plated carbon fiber chassis compared with the stainless steel-metal chassis can be as high as 71.43–76.25%.

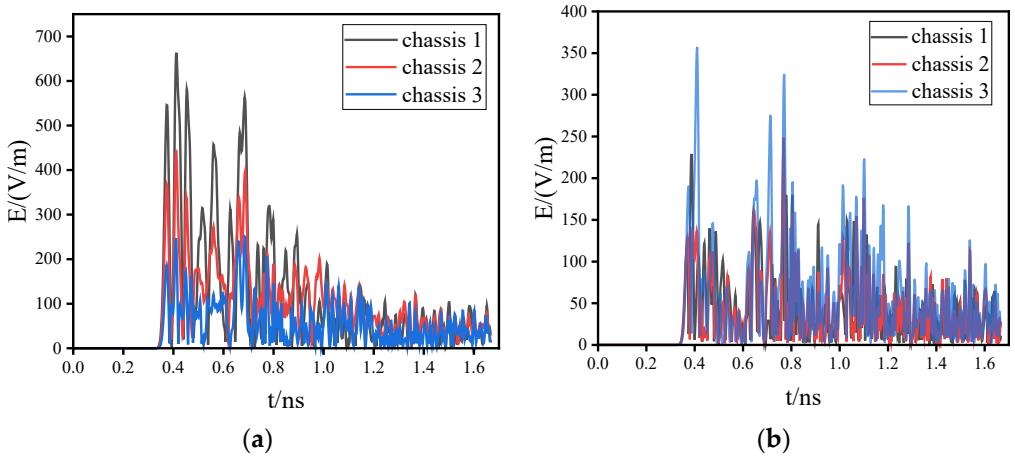

Figure 7. Electric field at the observation point of different structural chassis: (**a**) horizontal polarization; (**b**) vertical polarization.

Table 2. Chassis time-domain SE and weight analysis.

Material Time-Domain SE	Nickel-Plated Carbon Fiber	Carbon Fiber	Stainless Steels
chassis 1, $\alpha = 0°$/dB	37.54	30.17	31.34
chassis 2, $\alpha = 0°$/dB	41.11	30.46	33.23
chassis 3, $\alpha = 0°$/dB	46.13	30.44	42.59
chassis 1, $\alpha = 90°$/dB	47.62	34.24	39.49
chassis 2, $\alpha = 90°$/dB	46.13	33.97	40.72
chassis 3, $\alpha = 90°$/dB	43.23	34.24	37.46
density/g/cm^3	1.9–2.2	1.4–2	7.7–8

Table 3. Change in minimum temperature of shielding chassis surface.

Temperature Material	Initial/K	In 30 s/K	In 60 s/K	In 90 s/K	In 120 s/K	In 180 s/K
Metal	273	273	273	273	273	273
Nickel-Plated Carbon Fiber	273	273	274	275	276	278
Carbon Fiber	273	275	277	280	282	285

This meticulous examination, embodied in the simulation results, accentuates the nuanced differences in shielding effectiveness amongst the materials tested, highlighting the composite material's superior performance in mitigating electromagnetic interference. The findings affirm the potential of nickel-plated carbon fiber composites as lightweight yet effective shielding solutions, thereby paving the way for their application in domains where both weight efficiency and electromagnetic protection are paramount.

3.4. Heat Dissipation Analysis

The efficacy of heat dissipation stands as a critical characteristic for the performance of shielding chassis, a factor that cannot be overlooked in the design and evaluation of such systems. In this investigation, the COMSOL Multiphysics 6.1 simulation software plays a pivotal role in analyzing the thermal behavior of shielding chassis composed of three distinct materials. To ensure a controlled and uniform basis for comparison, each chassis was initialized at a surface and ambient temperature of 273 K. A consistent heat source, simulating the operational temperature typically encountered by a PCB board at 323 K, was

strategically positioned at the lower section of each chassis. This setup aimed to replicate real-world operating conditions closely, facilitating an accurate assessment of the materials' thermal management capabilities.

The outcomes of this simulation, specifically the spatial temperature distribution on the surfaces of the three types of shielding chassis after a three-minute exposure to the heat source, are meticulously illustrated in Figure 8. The color-coded temperature map provides an intuitive visual representation, with the numerical values at the top and bottom of the color scale indicating the maximum and minimum surface temperatures observed, respectively. A further detailed analysis of the temporal evolution of the surface temperature, particularly focusing on the minimum temperature fluctuations recorded during the three-minute period, is presented in Table 3.

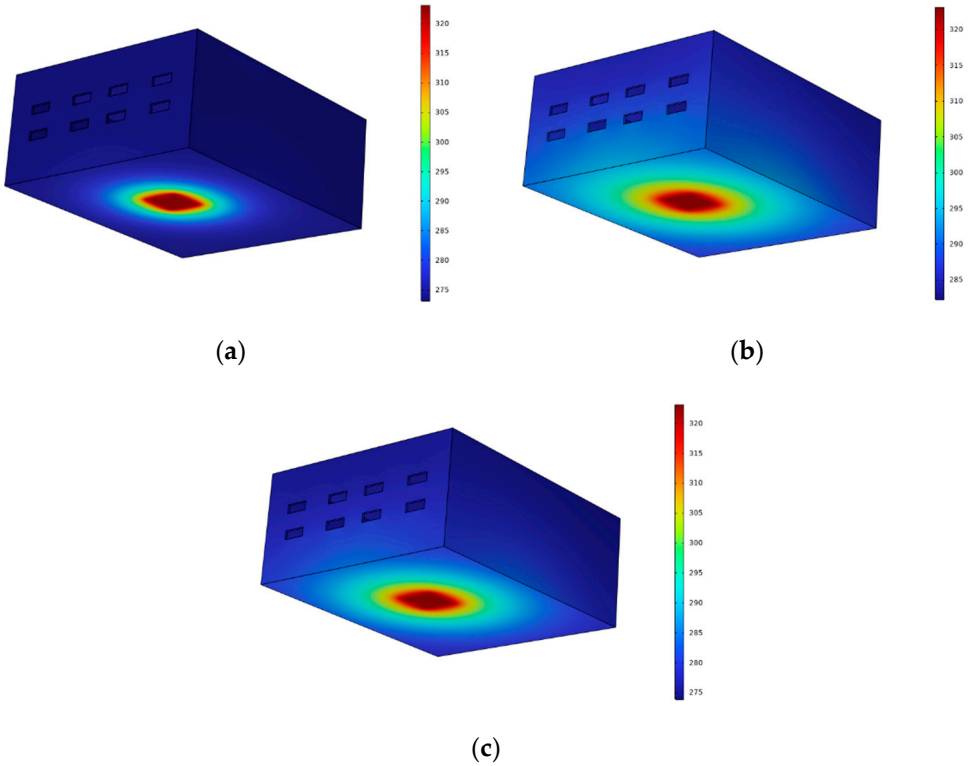

Figure 8. Shielding chassis's thermal analysis: (**a**) metal; (**b**) carbon fiber; (**c**) nickel-plated carbon fiber.

A comparison of the thermal performance of the three materials is shown in Figure 8 and Table 3. The metal chassis has the best heat dissipation ability, with its surface temperature initially set at 273 K and remaining constant for 180 s, allowing it to conduct heat to the outside world quickly. In contrast, the carbon fiber chassis shows the least cooling ability. From an initial temperature of 273 K, the temperature increased by about 2 K to 3 K between 60 and 180 s, for a total of 12 K in 180 s, making it slow to transfer heat to the outside world. The nickel-plated carbon fiber chassis, on the other hand, has great potential in terms of thermal performance, showing a small increase of 1 K or just over 1 K every 30 s from the initial reading to 180 s, demonstrating a significant increase in thermal performance over carbon fiber.

To summarize, the metal chassis comes a distant second in terms of heat dissipation, indicating the best thermal efficiency. Nickel-plated carbon fiber chassis comes in second, showing commendable thermal management capabilities, while carbon fiber chassis falls behind, showing the worst thermal performance. This analysis highlights the unique thermal properties of materials, providing insightful data on their suitability for applications where thermal management is critical.

4. Conclusions

In this investigation, a novel metallized carbon fiber composite material was developed, from which a lightweight electromagnetic shielding chassis boasting commendable shielding efficacy was engineered. Numerical simulations were utilized to compute the time-domain shielding effectiveness (SE) of chassis fabricated from metal, carbon fiber, and the newly developed composite, under varying different hole array structures and polarization modes. Additionally, comprehensive analyses concerning the weight and thermal dissipation capabilities of the chassis constructed from these three distinct materials were conducted. The following main conclusions were drawn from this study:

(1) In a double-shielded construction chassis, the newly designed lightweight electromagnetic shielding chassis provides better shielding performance than conventional metal-based counterparts. Notably, the chassis constructed from carbon fiber alone demonstrated the least effective electromagnetic shielding among the materials tested.
(2) In terms of weight, the lightweight carbon fiber composite chassis closely mirrors the carbon fiber chassis in heft. However, when benchmarked against the metal chassis, a significant weight reduction ranging between 71.43% and 76.25% was observed, highlighting the composite's advantage in lightweight design.
(3) Thermal analysis shows that the metal chassis has optimal thermal performance with negligible change in surface temperature, while the carbon fiber chassis has the fastest rise in temperature, slow heat conduction, and the worst thermal performance. Compared with the metal chassis, the surface temperature of the carbon fiber composite chassis increases slightly, but compared with the carbon fiber chassis, the thermal performance has a significant improvement.

These conclusions underscore the efficacy of the composite chassis developed in this study, which combines excellent electromagnetic shielding with notable advantages in weight reduction and thermal management. The findings validate the potential of metallized carbon fiber composites as superior materials for electromagnetic shielding applications. Furthermore, this research provides a solid foundation for the future application of carbon fiber composites in electromagnetic protection and paves the way for the design of lightweight shielding enclosures capable of operating within complex electromagnetic environments.

Author Contributions: Conceptualization, L.C., G.-H.D. and X.-Q.L.; methodology, L.C., C.-Z.Y. and H.-W.Y.; validation, T.-Y.Z. and C.-Z.Y.; writing—original draft preparation, C.-Z.Y. and H.-W.Y.; writing—review and editing, L.C. and X.-Q.L. All authors have read and agreed to the published version of the manuscript.

Funding: This research was funded in part by the National Natural Science Foundation of China (Grants No. 62101433), China Postdoctoral Science Foundation (Grant No. 2019M653634), and Natural Science Basic Research Plan in Shaanxi Province of China (Grant No. 2019JQ-797).

Institutional Review Board Statement: Not applicable.

Informed Consent Statement: Not applicable.

Data Availability Statement: Data is contained within the article.

Conflicts of Interest: The authors declare no conflicts of interest.

References

1. Cao, L.; Hao, S.; Zhao, Y.; Wang, C. High-Power Electromagnetic Pulse Effect Prediction for Vehicles Based on Convolutional Neural Network. *Electronics* **2022**, *11*, 1490. [CrossRef]
2. Park, Y.-J.; Pan, R.; Montgomery, D.C. Analysis of Electromagnetic Interference Effect on Semiconductor Scanning Electron Microscope Image Distortion. *Appl. Sci.* **2024**, *14*, 223. [CrossRef]
3. Gifuni, A.; Bastianelli, L.; Gradoni, G.; Moglie, F.; Perna, S.; Smartt, C.; Primiani, V.M. On the Shielding Effectiveness Calculation of Enclosures Through Measurements in Reverberation Chambers. *IEEE Trans. Electromagn. Compat.* **2021**, *63*, 1395–1406. [CrossRef]

4. Ramani, S.; Raby, E.Y.; Marksteiner, Q. Comparison Between Shielding Effectiveness of Slotted Cavities in a Mode Stirred Chamber and Free Space. *IEEE Trans. Electromagn. Compat.* **2023**, *65*, 943–953. [CrossRef]
5. Clerico, P.; Pichon, L.; Mininger, X.; Dubrunfaut, O.; Monsef, F.; Gannouni, C.; He, D.; Bai, J.; Prevond, L. Assessment of Broadband Shielding Effectiveness of Composite Panels for Protective Enclosures. *IEEE Trans. Electromagn. Compat.* **2022**, *64*, 1750–1757. [CrossRef]
6. Long, S.; Timothy, C.W.L.; Chinnici, A.; Graham, J.N. The Flow-Field within a Vortex-Based Solar Cavity Receiver with an Open Aperture. *Exp. Therm. Fluid Sci.* **2021**, *123*, 110314. [CrossRef]
7. Guo, J.W.; Ma, L.; Bi, X.G.; Dong, G.F.; Li, Y.G.; Ning, J.; Wu, K. X-band TE101 Rectangular Aperture Cavity for In Vivo EPR Tooth Dosimetry after Radiation Emergency. *Appl. Radiat. Lsotopes* **2021**, *178*, 109958. [CrossRef] [PubMed]
8. Cao, L.; Xie, Y.Z.; Gao, M.X. Analysis of Time-domain Shielding Effectiveness of Enclosures Above Lossy Half-space Using an Improved Half-space FDTD Method. *IEEE Trans. Electromagn. Compat.* **2020**, *62*, 2076–2083. [CrossRef]
9. Budumuru, S.; Rao, S.S.; Jenjeti, D.; Apparao, V.S. Shielding Effectiveness of Multilayer Laminate of Aluminum Metal Matrix and Micro Absorbing Materials. *MethodsX* **2023**, *10*, 102172. [CrossRef] [PubMed]
10. Eriksson, G.; Salinas, E. Shielding Properties of Welded and Unwelded Wire Mesh Enclosures. *IEEE Trans. Electromagn. Compat.* **2022**, *64*, 1703–1707. [CrossRef]
11. Yang, F.; Ma, S.C.; Khor, C.M.; Su, Y.M.; Barani, Z.; Barani, Z.P.; Boyko, A.; Iddya, A.; Segev-Mark, N.; Zheng, X.; et al. One-step Method for the Fabrication of Pure and Metal-decorated Densified CNT Films for Effective Electromagnetic Interference Shielding. *Carbon* **2023**, *214*, 118370. [CrossRef]
12. Firdosy, S.; Ury, N.; Dang, K.; Narvaez, P.; Dillon, R.P.; Ravi, V.A. Additively Manufactured High Permeability Fe-Ni Alloys and Novel Bi-metallic Magnetic Shields. *J. Magn. Magn. Mater.* **2023**, *584*, 171049. [CrossRef]
13. Zhao, Q.; Zhang, K.; Zhu, S.; Xu, H.; Cao, D.; Zhao, L.; Zhang, R.; Yin, W. Review on the Electrical Resistance/Conductivity of Carbon Fiber Reinforced Polymer. *Appl. Sci.* **2019**, *9*, 2390. [CrossRef]
14. Fang, Y.Q.; Zheng, G.W.; Bai, Y.J.; Zhang, T.N.; Wang, Y.H. Lightweight Structure Design and Heat Dissipation Research of High-strength Carbon Fiber Fully Sealed Case. *Fiber Comp.* **2022**, *108*, 108–113.
15. Savi, P.; Ruscica, G.; di Summa, D.; Natali Sora, I. Shielding Effectiveness Measurements of Drywall Panel Coated with Biochar Layers. *Electronics* **2022**, *11*, 2312. [CrossRef]
16. Yoo, J.; Lee, S. Experimental Study on Electromagnetic Shielding Characteristics of a Fe-Based Amorphous Soft Magnetic Composite. *Appl. Sci.* **2022**, *12*, 6158. [CrossRef]
17. Zhang, X.Z.; Wang, J.C.; Yang, S.L.; Feng, H.X. The Growth of In-situ CNTs on Slag to Enhance Electromagnetic Interference Shielding Effectiveness of Cement-based Composite. *Constr. Build. Mater.* **2024**, *411*, 134643. [CrossRef]
18. Chen, J.; Wu, J.; Ge, H.; Zhao, D.; Liu, C.; Hong, X. Reduced Graphene Oxide Deposited Carbon Fiber Reinforced Polymer Composites for ElectroMagnetic Interference Shielding. *Compos. Part A Appl. Sci. Manuf.* **2016**, *82*, 141–150. [CrossRef]
19. Amaro, A.; Suarez, A.; Tamburrano, A.; Torres, J.; Marra, F.; Martinez, P.A.; Galindo, B.; Soriano, N.; Victoria, J.; Alcarria, A. EMI Shielding Effectiveness Study for Innovative Carbon Nanotube Materials in the 5G Frequency Region. *IEEE Trans. Electromagn. Compat.* **2023**, *65*, 177–185. [CrossRef]
20. Zhu, C.; Li, R.; Chen, X.; Chalmers, E.; Liu, X.; Wang, Y.; Xu, B.B.; Liu, X. Ultraelastic Yarns from Curcumin-Assisted ELD Toward Wearable Human–Machine Interface Textiles. *Adv. Sci.* **2020**, *7*, 2002009. [CrossRef] [PubMed]
21. Araneo, R.; Celozzi, S. *Toward a Definition of the Shielding Effectiveness in the Time–Domain*; 2013 IEEE EMC Symposium: Denver, CO, USA, 2013; pp. 113–117.

Disclaimer/Publisher's Note: The statements, opinions and data contained in all publications are solely those of the individual author(s) and contributor(s) and not of MDPI and/or the editor(s). MDPI and/or the editor(s) disclaim responsibility for any injury to people or property resulting from any ideas, methods, instructions or products referred to in the content.